# Three-Dimensional Fluidic Self-Assembly by Axis Translation of Two-Dimensionally Fabricated Microcomponents in Railed Microfluidics

Su Eun Chung, Yoonseok Jung, and Sunghoon Kwon\*

**A** method for high-throughput 3D self-assembly of 2D photopatterned microstructures using railed microfluidics is presented. Vertical device patterning of heterogeneous materials requires high-level integration using conventional microelectromechanical system (MEMS) technology; however, 3D railed assembly enables easy and fast self-assembly via a fluidic axis-translation process and simple material exchange in microfluidic channels. Individually photopatterned 2D microstructures are axistranslated from in-plane to out-of-plane and fluidically self-assembled, guided by side-rails in microfluidic channels to form a 3D morphology. Since the structures are fabricated in fluidic environments, there are no fixed initial points on the channel substrate allowing fluidic horizontal stacking of erected 2D structures. The guiding mechanism of railed microfluidics enables efficient fluidic handling and deterministic 3D self-assembly of heterogeneous components such as electronic components or polymeric microstructures using only fluidic force.

#### 1. Introduction

Self-assembly is a promising pathway for parallel fabrication of devices made up of small components.<sup>[1]</sup> All the components are assembled together after the initial fabrication by suitable driving forces, such as gravity, [2-4] surface energy, [5] electrostatic force, [6] electromagnetic force, [7] fluidic force, [8,9] or capillary force. [10,11] A variety of applications are introduced to self-assemble heterogeneous materials, for example, light-emitting diodes (LEDs) on a silicon substrate<sup>[4]</sup> or a flexible substrate, [12] radio-frequency identification (RFID) chips on antennas, [13] bead packing on a patterned glass substrate<sup>[14]</sup> and so on. Such self-assembly techniques are often massively parallel and therefore can be scaled to increase speed and reduce cost. However, assembly yield is not as high owing to the probabilistic nature of self-assembly. Increasing the chance of components meeting together is critical to increase assembly yield. As demonstrated in fluidic selfassembly (FSA) of RFID<sup>[2]</sup> or assembly of DNA origami,<sup>[15]</sup> this is often done by overloading the number of parts floating around the assembly sites to increase the probability of matching and assembling. Thus, unnecessary mass production of microcomponents is required in most FSA processes. However, if microstructures could be accurately guided in a fluidic environment, an efficient FSA process combining the advantages of high-yield robotic assembly and high-throughput FSA would be achieved.

As an accurate guided self-assembly process, electric fields are often used to assemble colloidal particles such as polystyrene and silica particles in liquid suspensions.<sup>[16]</sup> Template-assisted guided self-assemblies have also been investigated using chemically treated surface templates<sup>[17,18]</sup> or electronically coupled semiconductor device layers<sup>[19]</sup> to assemble various components. Recently, railed microfluidics has been developed<sup>[20]</sup> as an ultimate guided self-assembly process. It is a deterministic way of assembling small and

S. E. Chung, Y. Jung, Prof. S. Kwon School of Electrical Engineering and Computer Science College of Engineering #066, and Inter-university Semiconductor Research Center (ISRC) Seoul National University 599 Gwanangno, Gwanak-gu, Seoul 151-744, South Korea E-mail: skwon@snu.ac.kr

DOI: 10.1002/smll.201001806

small ...

discrete heterogeneous components accurately without an error in a fluidic environment. However, a 3D guided and FSA process using railed microfluidics has not yet been reported.

Of interest is a deterministic 3D selfassembly of heterogeneous microstructures in a fluidic environment by expanding 2D railed microfluidics technique. Most 3D self-assembly processes are executed by capillary force or surface energy minimization<sup>[21-25]</sup> in liquid environments. In addition to the capillary-based 3D self-assembly conventional microelectromethods, mechanical system (MEMS) technology applied for microgripper-assisted assembly<sup>[26]</sup> or hinged assembly.<sup>[27,28]</sup> 2D fabricated structures are initially fixed on the substrate and translated from in-plane to out-of-plane centering on the fixed points. Since vertical patterns of the final 3D morphology are controlled during 2D fabrication, hinged self-assembly enables complex 3D shape formation. However, the procedure is complicated and timeconsuming, and all the initial points are fixed on the substrate causing the assembly to be executed only in a purposed manner. Furthermore, these methods are focused on structures with a single material composition rather than heterogeneous mate-

rials because heterogeneous vertical patterning requires very complex integration steps.

Herein, we demonstrate a 3D railed self-assembly using an axis-translation technique to move structures from inplane to out-of-plane. By combining this axis-translation concept of MEMS-based 3D assembly with the FSA process, railed microfluidics is expanded from a 2D to a 3D assembly technology. All the microstructures are fabricated in two dimensions, thus guided self-assembly is achieved by 2D railed microfluidics first, and then fluidically erected from the xy plane to the xz plane. After the structures are made to stand, the axis-translated 2D structure is guided by side rails, and then horizontally stacked sequentially by the fluidic force. Since there is no fixed initial point of the microstructures on the substrate, we easily handle the 2D patterned structures using the guiding mechanism of railed microfluidics. Also, guided microstructures are deterministically self-assembled in liquid environments, which overcomes the limitation of previous 3D FSA techniques. With this method, various 3D FSA and heterogeneous vertical patterning processes are demonstrated.

#### 2. Results and Discussion

**Figure 1** a schematically illustrates the experimental setup of the side-railed microfluidic system for 3D self-assembly, which combines a railed microfluidic channel<sup>[20]</sup>

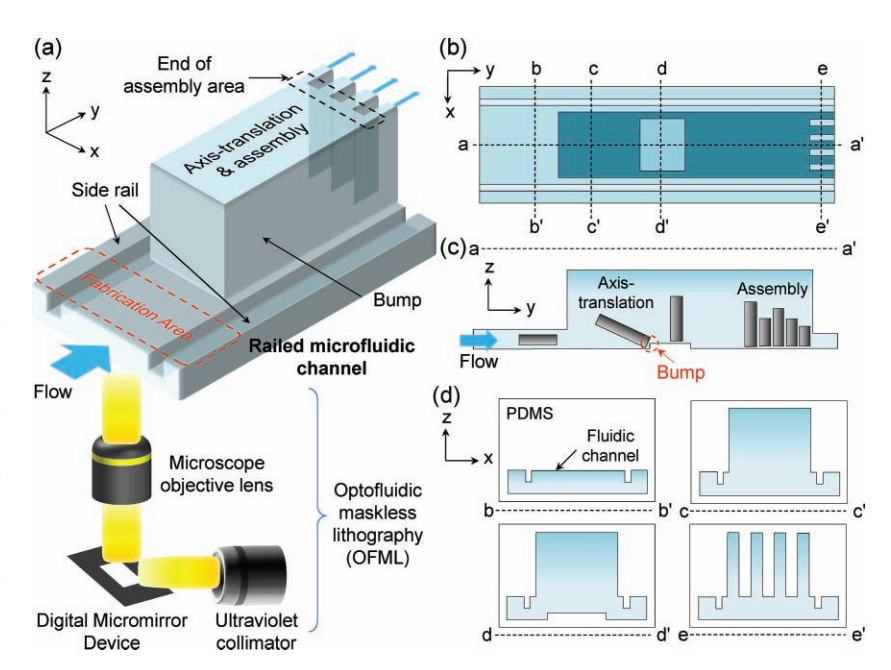
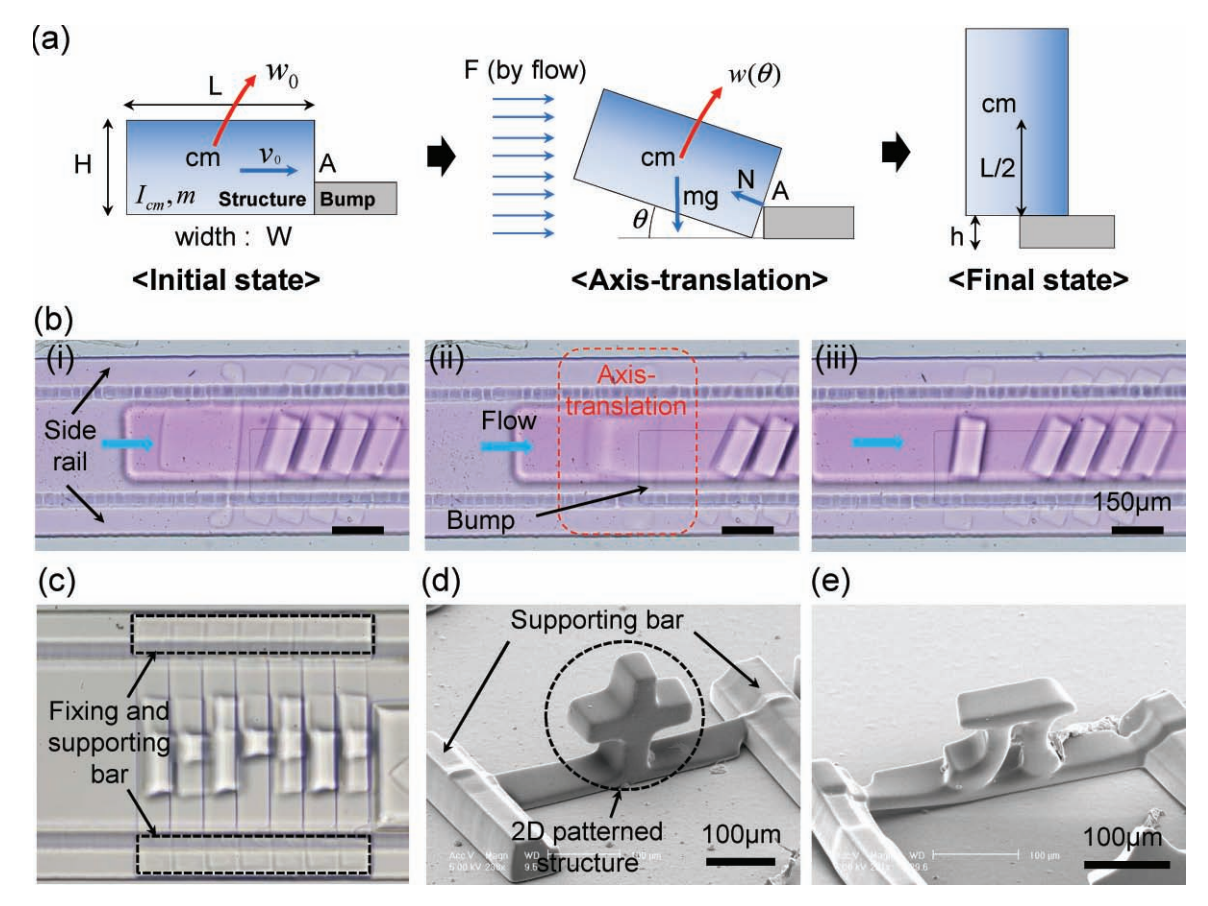


Figure 1. Microfluidic channel design for 3D railed self-assembly. a) Schematic diagram of a railed microfluidic channel with side rails for self-assembly of 2D patterned microstructures. The 2D microstructures are formed in the fabrication area along the xy plane using an OFML setup. The structure flows to the axis-translation and assembly area and rotates to the z axis in 90° at a bump embedded at the bottom of the channel. Side rails are used to guide fabricated structures during the rotation and assembly process. b) Top view of the side-railed microfluidic channel (xy plane). The darkest blue corresponds to the deepest part of the channel. c) Cross-sectional view of the channel (yz plane) cut at yz plane) cut at yz plane) cut at yz plane cut at yz plane cut at yz plane e-yz from (yz plane). PDMS = polydimethylsiloxane.

and optofluidic maskless lithography (OFML) system.<sup>[29]</sup> In OFML, UV-curable resin flowing in the channel is photopolymerized through dynamic projection patterns modulated from the digital micromirror device (DMD, Texas Instruments). The top view of the polymerized microstructure is defined by the exposure pattern of the UV light from the DMD, thus various microstructures with arbitrary 2D patterns are easily fabricated via OFML.

The key of 3D railed self-assembly is the design of the railed microfluidic channel. Instead of rails on top of the microfluidic channels, we used side rails as described in Figure 1a. Side-railed microfluidic channels are divided into two areas: the fabrication area (80 µm depth) and the assembly area (520 µm depth). In the fabrication area, 2D microstructures are photopatterned along the xy plane via OFML. The channel has common side-guiding rails on both sides to move fabricated structures along the rail from the fabrication region to the assembly region. 2D synthesized structures in the fabrication area are fluidically transferred to the assembly area through guidance along the side rails, and then rotate by 90° at the bump embedded at the bottom of the channel due to continuous fluidic force. In this way, individually fabricated 2D microstructures with various patterns are vertically assembled within the deep assembly region at the end of the rails. Since all the arbitrary photopatterned 2D structures are standing upright during the assembly, the final structure has various vertical patterns which cannot be easily produced using conventional lithography.

full papers



**Figure 2.** Axis translation in a side-railed microfluidic channel. a) Modeling of the axis-translation process. The structure starts to rotate for H > 2h and the angular speed increases as h reduces. b) Process of axis translation. i) Initial state. The fabricated 2D structure flows from left to right guided by side rails. ii) Axis translation. The structure stops at the bump and rotates  $90^{\circ}$  due to continuous fluidic force. iii) Final state. The axis-translated structure flows forward, guided along the side rails by the fins. Then, the structure is assembled in the horizontal direction. c) Fixation of 3D self-assembly. By exposing the bar-type pattern after the assembly, the fixing bar binds all assembled structures and supports them from collapse upon the removal of the fluidic channel. d,e) Axis-translated 2D patterned structures with supporting bars.

The channel used in the experiments has three different depths, as shown in Figure 1b–d. The brightness of the color in the xy-plane view represents the depth of the channel (Figure 1b). The darkest blue corresponds to the deepest part which is 520  $\mu$ m in depth. To cover all the arbitrary heights of the fabricated structures, the axis-translation and assembly area is significantly deeper than the fabrication area. Figure 1c shows the yz-plane view of the channel which is a cross section of the side-railed microfluidic channel in a parallel direction to the flow cut at a–a' from Figure 1b.

The bump at the bottom of the channel is a key to the axis translation of the 2D fabricated structure, which aids structural posturing. It is extruded in the z direction to aid axis translation of the flowing 2D structure. The 2D structure is made to stand upright by tripping over a bump, which results in axis translation due to continuous fluidic force in the y direction, as shown in Figure 1c. The flow pushes the axis-translated structure to move to the end of the assembly area, thus completing the assembly. Cross sections in the xz plane, which is an orthogonal direction to the flow cut at b-b', c-c', d-d', and e-e' from Figure 1b, show the depth difference of each part in the side-railed

microfluidic channel (Figure 1d). The cross section at b-b' shows the fabrication area. The heights of both the photopatterning region and side rails are the same. Cross sections at c-c' and d-d' are the axis-translation area. The cross section at d-d' shows a bump at the bottom of the channel. Finally, the cross section at e-e' is the end of the rails, which allows self-assembly of axis-translated 2D photopatterned structures. Detailed fabrication methods of this multistep side-railed microfluidic channel are described in the Experimental Section. The side-railed microfluidic channel is used to self-assemble fabricated 2D layers with various patterns in the vertical direction to make the final 3D structure.

For the structure to fully stand up, it must have enough initial energy, which results from the fluidic force, to overcome the force of gravity enacted upon it. Theoretically, the property in axis translation of the structure can be expected approximately from the following equations. The morphology of the 2D patterned structure determines a rotational inertia at the center of mass,  $I_{\rm cm}$ . At the instant of collision between the flowing 2D structure and the bump, angular momentum J is conserved at point A as follows (Equation (1) and **Figure 2**a):



$$J = m v_0 \left(\frac{H}{2} - h\right)$$

$$= \left(I_{cm} + m\frac{L^2}{4} + m\left(\frac{H}{2} - h\right)^2\right) w$$
(1)

where m is the mass of the structure,  $v_0$  is the structure velocity, H is the height of the 2D patterned structure, h is the height of a bump, L is the length of the 2D patterned structure, and w is the angular speed. Due to the conservation of angular momentum at point A, the initial angular speed  $w_0$  is:

$$w_0 = \frac{m(\frac{H}{2} - h)}{I_{\rm cm} + m(\frac{L^2}{4} + m(\frac{H}{2} - h)^2)} v_0$$
 (2)

From Equation (2), the structure starts to rotate when half of the structure height is higher than the height of the bump. When the center of mass of the structure is higher than the height of the bump, the structure collides with the bump. With the initial angular speed  $w_0$ , every motion of the structure starts to be governed by a fluidic frictional force due to low Reynolds number. Therefore, the structure should have a sufficient driving torque for the full axis translation by an external pressure to overcome the frictional torque exerted by the resin [Equation (3)]. For simplicity of the analysis, we assumed that the structure is rigid and the turbulence of the flow around the structure is negligible.

$$\frac{L}{2} \left( \frac{1}{2} \rho_{\text{liquid}} v_0^2 \right) L W \sin \theta > \frac{1}{L} \int_0^L \zeta r^2 w dr$$
 (3)

$$w \simeq \frac{v_0 \sin \theta}{L} \tag{4}$$

In Equation (3), the left-hand term is the driving torque by the external pressure applied to the structure, where  $\rho_{\text{liquid}}$  is the viscosity of the resin,  $v_O$  is the velocity of the liquid, W is the width of the 2D patterned structure, and  $\theta$  is the rotation angle. The right-hand term is a torque created by the frictional force, where  $\zeta$  is the frictional coefficient of the structure,  $\omega$  is the angular speed at an angle of  $\theta$ , and r is the radius from point A to the center of mass. Equation (4) indicates an assumption that the end-line of the axis-translating structure follows the flow of the resin.

By setting Equation (3) to be satisfied for every rotation angle, we can obtain the minimum pressure for the full axis translation as follows:

$$P(\text{minimum}) \simeq \frac{8\zeta^2}{9L^2W^2\rho_{\text{liquid}}}$$
 (5)

From Equation (2) and (5), we can get the appropriate height of the bump in a channel and minimum pressure required to axis-translate the 2D patterned structure.

OFML is a dynamic 2D polymeric microstructure fabrication method in microfluidic channels using a DMD. By combining the OFML technique with railed microfluidics, a powerful microstructure guiding and assembly technique

in a fluidic environment, various 2D microstructures are photopolymerized in situ and self-assembled forming a 3D morphology. As a proof-of-concept demonstration, we axistranslated 2D polymeric microstructures as shown in Figure 2b. In the initial state, the fabricated structure flows from left to right with the uncured polymer resin guided by side rails due to "fins" at both sides of each structure (Figure 2b(i)). At the bump, the flowing structure stops and rotates 90° in the y direction (Figure 2b(ii)). Continuous flow forces the structure to move against a viscous liquid solution and the gravity of the fabricated structure. After the axis translation, the structure moves forward guided along the side rails due to the fins, and then it is finally assembled in the horizontal direction. Therefore, the assembled structures have vertical patterns at the final state (Figure 2b(iii)). By making structures with various lengths along the horizontal plane, it is possible to have multiheight patterns in the final assembled form. All the 2D patterns are determined by the DMD patterns from the OFML system. Due to the dynamic lithography method, arbitrary patterns are fabricated for 2D structures to form the desired 3D assembly.

All the axis-translated structures are only stabilized while the resin is flowing forward, and they need supporters to remain standing outside of the channel. To fix the structures by binding them together, we expose a bar-type pattern on the fins of the structures after the assembly (Figure 2c). The fixing and supporting bar binds all the assembled structures, and supports the axis-translated structure not to collapse outside as well as inside the microfluidic channels. Before the structures were removed from the microfluidic channel, the assembly was completely washed out with buffer solution and dried while the structures were fixed at the end of the assembly area. After the structures were all dried, the microfluidic channel was removed from the PDMS substrate. Figure 2d and e show axis-translated 2D patterned structures from outside of the channel with supporting bars on both sides.

All the 2D shapes are determined by the DMD patterns from the OFML system; thus, this dynamic lithography method allows arbitrary patterns for 2D structures to form desired 3D assemblies. Since these 2D structures are axis-translated during the self-assembly process, the final structures have various vertical patterns. Using 3D railed selfassembly, we demonstrate various self-assembled structures in 3D with different vertical patterns. Figure 3a and b show the FSA of height-controlled structures. Using dynamic DMD lithography, the height of 2D photopatterned structures is controlled during the fabrication process. The heights of the structures either slightly increase or decrease (Figure 3a). Repeated height variation results in a sinusoidal wave-shaped fluorescence intensity profile, as shown in Figure 3b(iii). This intensity profile is derived from the fluorescence image of the final self-assembled structures, and is similar to a sine wave due to the varying height. By only changing 2D patterns via OFML and flowing the fabricated structures with the liquid, we easily self-assembled them and formed a 3D morphology.

To show the diverse generation of vertical patterns using 3D railed self-assembly, we formed a lateral surface stamp structure, as shown in Figure 3c. The lateral stamp assembly shows that assembled 2D structures are embossed with

full papers

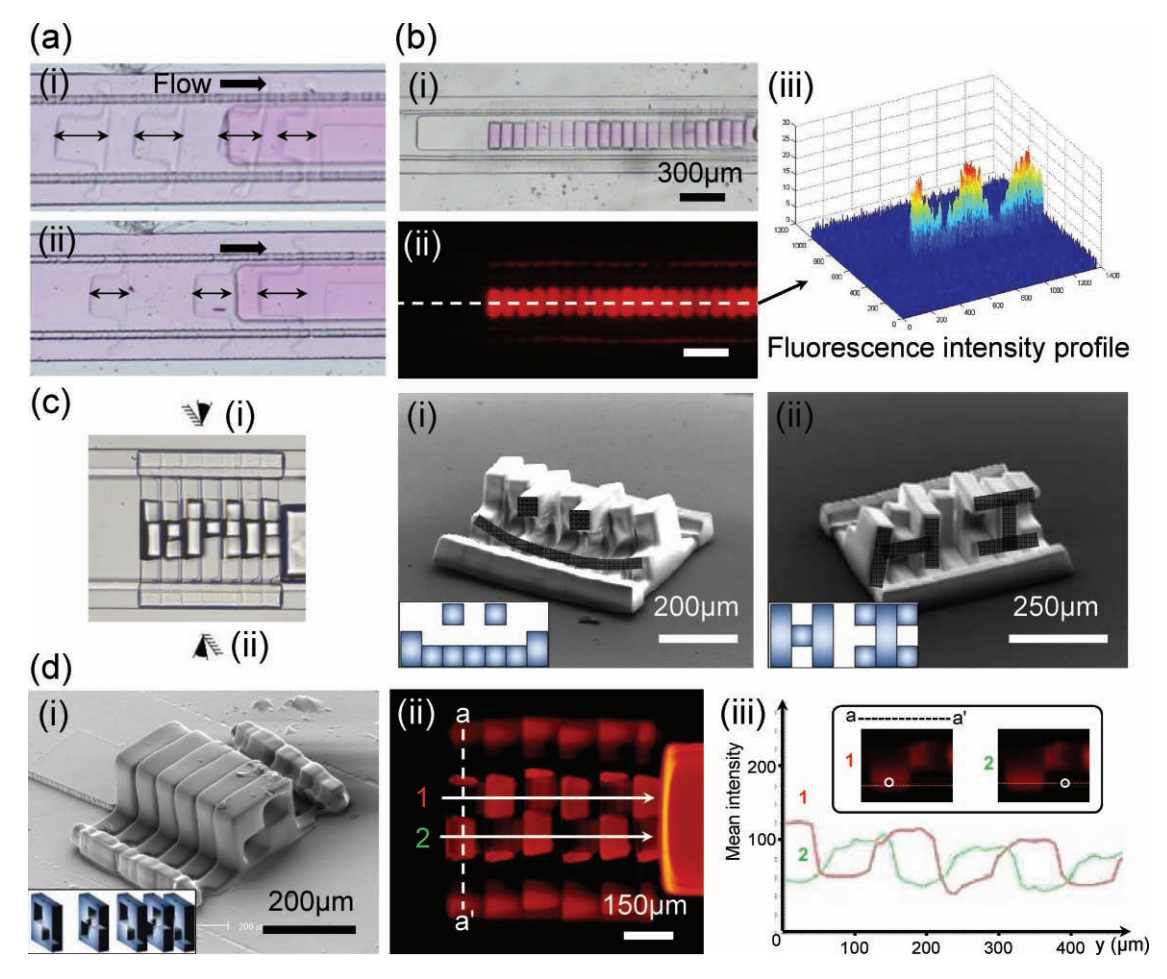


Figure 3. 3D railed self-assembly. a,b) Height-controlled structure self-assembly. Height of 2D patterns a) i) increase or ii) decrease, and b) finally all the axis-translated structures are horizontally assembled to form a height-controlled structure. b) i) Microscope image of self-assembled height-controlled structures. iii) Corresponding fluorescence microscopy image. iii) Fluorescence intensity profile analyzing the fluorescence image from (ii). c) Top microfluidic image of lateral surface stamp assembly. Two different lateral stamp patterns are shown on each side of the assembly. i) "SMILE" shape lateral pattern on one side. ii) "HI" shape characters on the other side of the final assembly. A single self-assembled structure has two different lateral patterns on each side by controlling the pattern of each 2D structure. d) Lattice assembly. i) Scanning electron microscopy (SEM) image. Each 2D part has a void cavity (inset). ii) Fluorescence microscopy image. iii) Confocal microscopy analysis of lattice assembly. The confocal microscope scans the cross section of the whole lattice assembly in a positive y direction to show alternating patterns starting at each white circle (starting point of scanning) in the cross-sectional image cut at a-a'. 1 (Red): The fluorescence intensity is high at y = 0. As scanning goes through the assembly, the intensity profile repeats high and low values due to the alternating patterns. 2 (Green): The fluorescence intensity is low at y = 0.

certain characters when viewed from the side. Two different lateral stamp patterns are generated on each side of the assembly (Figure 3c). The assembly is composed of seven axis-translated 2D structures all with different patterns to form a lateral stamp in the final assembled structure. Perspective views of the assembly are depicted as human eves on the microscopic image of self-assembled structures (Figure 3c). The left and right sides of the flow direction are shown in Figure 3c(i) and (ii), respectively. Figure 3c(i) shows a "SMILE" shape pattern and Figure 3c(ii) is a "HI" pattern. Finally, a single self-assembled structure has two different lateral patterns by controlling the pattern of each 2D structure. The lateral stamp assembly structure is not easy to fabricate with conventional MEMS technology. Our method takes just a few seconds including all the fabrication and assembly processes.

Fabricating a structure with a cavity, or a void area, is a very complicated and time-consuming process using conventional MEMS technology. It requires several steps of photolithography, etching, and development process to make one void area inside the structure. However, the 3D railed assembly technique enables fast and easy cavity fabrication simply by patterning 2D structures with a hole and flowing them within side-railed microfluidic channels to axistranslate and assemble them. As shown in Figure 3d, the void area exists inside assembled lattice structures. This assembly is composed of alternating lattice structures. Each 2D photopatterned part has two void cavities similar to a single set of checkered pattern, and the cavity parts in the pattern alternately and repeatedly change with noncavity parts as the fabrication process proceeds (inset of Figure 3d(i)). Figure 3d(i) is a SEM image showing alternating lattice structures and

small ...

Figure 3d(ii) shows a fluorescence microscopy image of assembled lattice structures. Confocal microscopy of the assembly is executed to confirm the presence of alternating vertical patterns throughout the entire assembly. As shown in Figure 3d(ii), the confocal microscope scans the cross section of the entire assembly in the direction of the two white arrows to prove the vertical lattice patterns. The scanning starts at each white circle in the confocal cross-sectional image of Figure 3d(iii) cut at a-a' from Figure 3d(ii). Since the first scan starts from the bottom-left part of the lattice pattern, which is a noncavity part (red 1 image), the analyzed graph (red 1 graph) proves that the fluorescence intensity is high at y = 0 showing full fluorescence. As scanning goes through the whole assembly, the intensity profile alternates between high and low due to the alternating cavity patterns. The second scan starts from the bottom-right part of the pattern, depicted as a white circle in the confocal microscopy image (green 2 image). The starting point of the scan is a cavity part, and thus the graph (green 2 graph) shows that the fluorescence intensity is low at y = 0, indicating that there is very weak fluorescence. The two graphs in Figure 3d(iii) have the opposite trend to each other, because one starts from a noncavity part and the other starts from a cavity part, and both go through alternate patterns repeatedly. These results

confirm that our 3D railed assembly method allows vertical cavity patterning.

The examples of self-assembly described above were demonstrated using microstructures made of the same polymeric material. However, the true advantage of guided self-assembly is in its capacity to assemble parts made out of different materials, or heterogeneous self-assembly. In conventional lithography, patterning two different materials in a single substrate requires two separate photolithography steps, two separate alignment steps, and two separate material patterning steps. In contrast, we have created a much simpler process to self-assemble microstructures made up of different materials by just introducing the solution alternately into the channel. This technique greatly simplifies heterogeneous patterning by eliminating multiple alignment and material deposition steps.

**Figure 4** shows the 3D self-assembly of heterogeneous materials. The pyramid-shaped 3D self-assembly product is composed of green and red blocks (Figure 4a). This assembly is made of five axis-translated (vertical) layers which are 2D patterned structures. Odd layers and even layers are different materials from each other. Since each vertical layer is composed of different materials, horizontal layers of the final assembly are heterogeneous patterns. Each 2D patterned structure for each layer is shown in Figure 4b. The first and fifth vertical

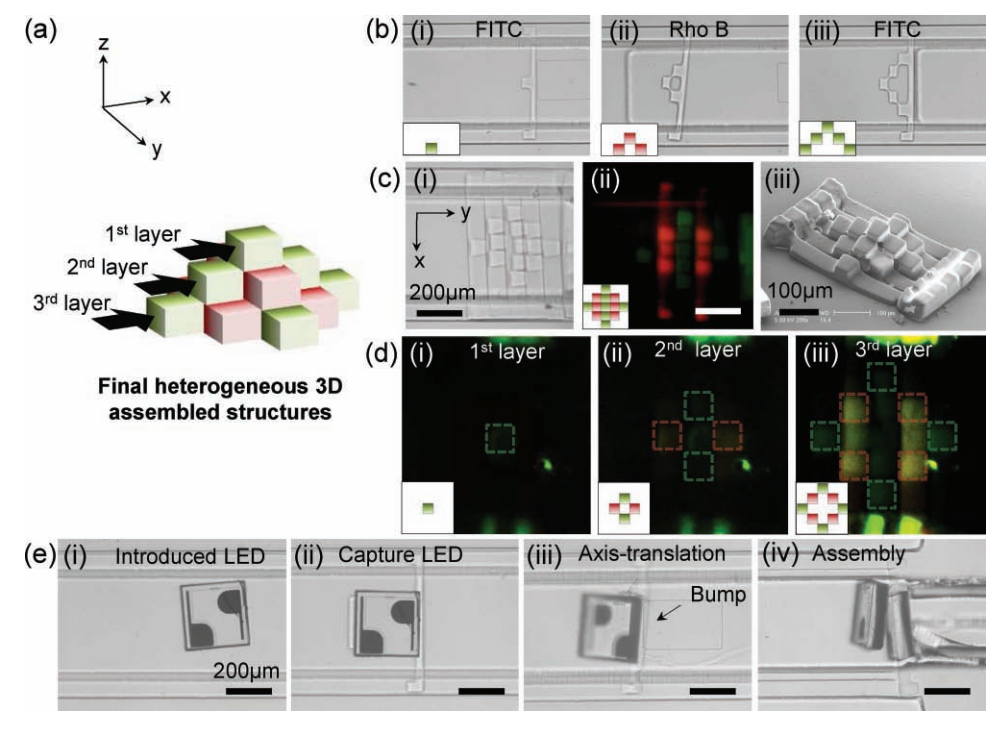


Figure 4. Heterogeneous 3D self-assembly. a) Schematic diagram of final pyramid-shaped 3D self-assembly composed of green and red blocks. The structure is made of five axis-translated (vertical) layers. Odd layers and even layers are made of different materials. b) 2D patterned structures for each solution. i) First and fifth vertical layers are made of fluorescein (FITC)-labeled PEG-DA. ii) Second and fourth vertical layers are made of rhodamine B (Rho B)-labeled PEG-DA. iii) The third vertical layer is made of FITC-labeled PEG-DA. c) Final assembled heterogeneous 3D structure. i) Top microscopy image of the final assembled structures. ii) Corresponding fluorescence image. iii) SEM image of the final pyramid-shaped 3D assembly. d) Confocal microscopy images of each horizontal layer denoted as in (a). i) First layer. Only the top block of the third vertical layer is shown as green fluorescence. ii) Second heterogeneous layer. The top blocks of the second and fourth vertical layers and second-top blocks of the third layer are shown as red and green fluorescence, respectively. iii) Third heterogeneous layer. Bottom blocks of all five vertical layers are shown. e) LED axis translation and self-assembly. Externally introduced LEDs are captured via the OFML system and assembled in side-railed microfluidic channels. i) Externally introduced LED mixed with polymer solution. ii) LEDs are captured by the OFML system and pushed along the side rails. iii) Axis-translation of the LED at the bump. iv) The erected LED is assembled at the end of the rail.

# full papers

layers are made of fluorescein (FITC)-labeled poly(ethylene glycol) diacrylate (PEG-DA; Figure 4b(i)). The second and fourth vertical layers are made of rhodamine B-labeled PEG-DA (Figure 4b(ii)). The third vertical layer is made of FITC-labeled PEG-DA (Figure 4b(iii)). Since the layers are made of different materials, the vertically assembled 3D structure has heterogeneous patterns. The fluorescence image of the final assembled pyramid-shape structure shows alternating red and green fluorescence for each layer (Figure 4c(ii)). Red and green fluorescence represent rhodamine B- and FITClabeled PEG-DA, respectively. Confocal microscopy images of each horizontal layer denoted as in Figure 4a show that each layer is composed of heterogeneous materials. The first layer is only the top block of the third vertical layer, shown as green fluorescence (Figure 4d(i)). The second layer is composed of two green blocks and two red blocks (Figure 4d(ii)), and the final horizontal heterogeneous layer is composed of all bottom blocks of five vertical layers (Figure 4d(iii)).

3D railed microfluidics also has applicability in industrial processes such as vertical LED chip assembly. Externally introduced LEDs are captured by the OFML system and assembled in side-railed microfluidic channels. The LEDs are mixed with polymer solution and introduced into the microfluidic channels (Figure 4e(i)). The LED flowing inside the channel is packaged by the OFML system in the fabrication region and moves along the side rails to the assembly area (Figure 4e(ii)). The rail-guided LED is axis-translated at the bump (Figure 4e(iii)), and then finally assembled at the end of the rails (Figure 4e(iv)). Rather than 2D self-assembly of a micrometer-scale device in railed microfluidics.<sup>[30]</sup> vertically stacked devices in the horizontal direction obtained by 3D railed self-assembly can be applied to various MEMS devices.

#### 3. Conclusion

In summary, we have developed a 3D self-assembly method using axis translation of 2D structures in railed microfluidic channels. Diverse self-assemblies are executed within a few seconds simply by repeating 2D patterning and rotational assembly of the structure in solution. 3D self-assembly of heterogeneous materials with different patterns resulting in different vertical assemblies is demonstrated, thus increasing the versatility of the railed microfluidics technique. Our method provides a fast and simple way to assemble various materials in three dimensions with low manufacturing cost.

### 4. Experimental Section

Optofluidic Maskless Lithography (OFML) Setup: An OFML system was used for photopolymerization. In the OFML setup, a high-intensity mercury-xenon lamp (200 W bulb) was used for ultraviolet photopatterning, combined with a digital micromirror device (DMD; Texas Instruments) to dynamically control the shape of the magnetic actuators. Exposure patterns on the DMD were controlled by a computer program (LabVIEW). An Olympus IX71 optical microscope was manually equipped with an ultraviolet lamp and DMD. A 10× microscope objective lens with a numerical aperture (NA) of 0.28 projected the computer-controlled image pattern on the MEMS spatial light modulator to the final object plane, with a demagnification factor of approximately 8.9. Because the pitch of the micromirror array was 13.68 um in the spatial light modulator plane, the pixel size in the object plane was approximately  $1.54 \mu m \times 1.54 \mu m$ . Visual alignment for photopolymerization was observed with a charge-coupled device (CCD) camera (DP71).

Materials: Poly(ethylene glycol) diacrylate (PEG-DA, Sigma-Aldrich,  $M_n = 258$ ) with 10 wt% photoinitiator (2,2-dimethoxy-2-phenylacetophenone) was used to synthesize polymeric structures. For the experiments with fluorescence microscopy, 3 mm rhodamine B (Sigma-Aldrich) and 3 mm FITC (Sigma-Aldrich) in PEG-DA solutions were used.

Fabrication of Microfluidic Device: A railed microfluidic device with three steps was used to fabricate 2D patterned structures and self-assemble in 3D. The microfluidic channels were prepared using standard photolithography and soft lithography methods. Photolithography processes were executed four times for 40, 40, and 520 µm heights. SU-8 photoresist (Microchem) was first spin-coated on a silicon wafer. It was then baked at 95 °C on a hotplate. Each layer was patterned through a film photomask (designed by AUTOCAD) of 25 000 dpi resolution and post-baked at 95 °C on a hotplate. The patterned wafer was then developed in an SU-8 developer. For a three-layer microfluidic channel with a groove structure, which was a side-railed microfluidic channel, a three-layer mold fabrication process was used by repeating this photolithography step in the mold preparation phase three more times. SU-8 2015 was used for the first two 40-um layers, and SU-8 2050 for next 520 um. The 520-µm-thick layer was for the axis translation and assembly and it was photopatterned twice using SU-8 2050 to fabricate deep parts under the same conditions. Another one-layer lithography process on a silicon wafer was executed using SU-8 2015 (15 µm thickness) for the bump layer, which was bonded to the side-railed microfluidic channel. Finally, two patterned wafers were hardbaked for 10 min at 110 °C on a hotplate. For the soft lithography process, each mold was transferred to PDMS silicon elastomer (Sylgard 184, Dow Corning) with 10 wt% of curing agent by baking for 15 min on a hotplate at 150 °C. Then, the fluidic channel was cut and punched at each inlet and outlet, and the bump layer was also cut. Next, two replica PDMS molds were bonded to each other by a plasma cleaning process for 20 s under a vacuum at 500-1000 mbar with a Plasma Cleaner PDC-32G (Harrick Plasma) to complete the microfluidic channel fabrication process.

#### Supporting Information

Supporting Information is available from the Wiley Online Library or from the author.

## *Acknowledgements*

This work was partly supported by KESRI (2009-F-020-01, 10031821, 10030573), which is funded by MKE (Ministry of Knowledge Economy) and partly supported by the Korea Science and Engineering Foundation (KOSEF) grant funded by the Korea government (MEST; 2010-0017860).



- [1] G. M. Whitesides, B. Grzybowski, Science 2002, 295, 2418.
- [2] E. J. Snyder, J. Chideme, G. S. W. Craig, Jpn. J. Appl. Phys. 2002, 41, 4366.
- [3] A. D. Ormonde, E. C. M. Hicks, J. Castillo, R. P. V. Duyne, *Langmuir* 2004, 20, 6927.
- [4] H. J. Yeh, J. S. Smith, IEEE Photonic. Tech. Lett. 1994, 6, 706.
- [5] D. Dendukuri, T. A. Hatton, P. S. Doyle, *Langmuir* **2007**, *23*, 4669.
- [6] J. J. Boote, K. Critchley, S. D. Evans, J. Exp. Nanosci. 2006, 1, 125.
- [7] M. Tanase, D. M. Silevitch, A. Hultgren, L. A. Bauer, P. C. Searson,
   G. J. Meyer, D. H. Reich, J. Appl. Phys. 2002, 91, 8549.
- [8] S. A. Stauth, B. A. Parviz, Proc. Natl. Acad. Sci. USA 2006, 103, 13922.
- [9] Y. Huang, X. Duan, Q. Wei, C. M. Lieber, Science 2001, 291, 630.
- [10] N. Bowden, A. Terfort, J. Carbeck, G. M. Whitesides, *Science* 1997, 276, 233.
- [11] U. Srinivasan, D. Liepmann, R. T. Howe, J. Microelectromech. Syst. 2001, 10, 17.
- [12] H. O. Jacobs, A. R. Tao, A. Schwartz, D. H. Gracias, G. M. Whitesides, *Science* **2002**, *296*, 323.
- [13] J. S. Smith, US Patent Patent No. 6611237, 2003.
- [14] Y. Lu, Y. Yin, Y. Xia, Adv. Mater. 2001, 13, 34.
- [15] P. W. K. Rothemund, Nature 2006, 440, 297.
- [16] W. D. Ristenpart, I. A. Aksay, D. A. Saville, Phys. Rev. Lett. 2003, 90, 128303.
- [17] S. Liu, R. Maoz, G. Schmid, J. Sagiv, Nano Lett. 2002, 2, 1055.
- [18] X. Xiong, Y. Hanein, J. Fang, Y. Wang, W. Wang, D. T. Schwartz, K. F. Bohringer, J. Microelectromech. Syst. 2003, 12, 117.

- [19] J. Liu, T. Lee, D. B. Janes, B. L. Walsh, M. R. Melloch, J. M. Woodall, R. Reifenberger, R. P. Andres, Appl. Phys. Lett. 2000, 77, 373.
- [20] S. E. Chung, W. Park, S. Shin, S. A. Lee, S. Kwon, *Nat. Mater.* 2008, 7, 581.
- [21] A. H. Cannon, Y. Hua, C. L. Henderson, W. P. King, J. Micromech. Microeng. 2005, 15, 2172.
- [22] J. Guan, H. He, D. J. Hansford, L. J. Lee, J. Phys. Chem. B 2005, 109, 23134.
- [23] T. L. Breen, J. Tien, S. R. J. Oliver, T. Hadzic, G. M. Whitesides, Science 1999, 284, 948.
- [24] D. H. Gracias, J. Tien, T. L. Breen, C. Hsu, G. M. Whitesides, Science 2000, 289, 1170.
- [25] W. Zheng, P. Buhlmann, H. O. Jacobs, Proc. Natl. Acad. Sci. USA 2004, 101, 12814.
- [26] N. Dechev, W. L. Cleghorn, J. K. Mills, J. Microelectromech. Syst. 2004, 13, 176.
- [27] E. E. Hui, R. T. Howe, M. S. Rodgers, presented at the 13th Ann. Intl. Conf. Microelectromechanical Syst., Japan, January 2000.
- [28] K. F. Harsh, V. M. Bright, Y. C. Lee, Sens. Actuators A 1999, 77, 237.
- [29] S. E. Chung, W. Park, H. Park, K. Yu, N. Park, S. Kwon, Appl. Phys. Lett. 2007, 91, 041106.
- [30] S. E. Chung, S. A. Lee, J. Kim, S. Kwon, Lab Chip 2009, 9, 2845.

Received: October 12, 2010 Revised: November 23, 2010 Published online: February 15, 2011